Journal of Photonics for Energy

PhotonicsforEnergy.SPIEDigitalLibrary.org

Bridging the p-type transparent conductive materials gap: synthesis approaches for disperse valence band materials

Angela N. Fioretti
Monica Morales-Masis

SPIE.

Angela N. Fioretti, Monica Morales-Masis, "Bridging the p-type transparent conductive materials gap: synthesis approaches for disperse valence band materials," *J. Photon. Energy* **10**(4), 042002 (2020), doi: 10.1117/1.JPE.10.042002

Bridging the p-type transparent conductive materials gap: synthesis approaches for disperse valence band materials

Angela N. Fioretti[a] and Monica Morales-Masis[b,*]
[a]Ecole Polytechnique Fédérale de Lausanne, Photovoltaics and Thin Film Electronics Laboratory, Neuchâtel, Switzerland
[b]University of Twente, MESA+ Institute for Nanotechnology, Enschede, The Netherlands

Abstract. Transparent conductive materials (TCMs) with high p-type conductivity and broadband transparency have remained elusive for years. Despite decades of research, no p-type material has yet been found to match the performance of n-type TCMs. If developed, the high-performance p-type TCMs would lead to significant advances in a wide range of technologies, including thin-film transistors, transparent electronics, flat screen displays, and photovoltaics. Recent insights from high-throughput computational screening have defined design principles for identifying candidate materials with low hole effective mass, also known as disperse valence band materials. Particularly, materials with mixed-anion chemistry and nonoxide materials have received attention as being promising next-generation p-type TCMs. However, experimental demonstrations of these compounds are scarce compared to the computational output. One reason for this gap is the experimental difficulty of safely and controllably sourcing elements, such as sulfur, phosphorous, and iodine for depositing these materials in thin-film form. Another important obstacle to experimental realization is air stability or stability with respect to formation of the competing oxide phases. We summarize experimental demonstrations of disperse valence band materials, including synthesis strategies and common experimental challenges. We end by outlining recommendations for synthesizing p-type TCMs still absent from the literature and highlight remaining experimental barriers to be overcome. [DOI: 10.1117/1.JPE.10.042002]

Keywords: transparent conductors; p-type; thin films; inorganic; materials; optoelectronics.

Paper 19095SSMV received Nov. 1, 2019; accepted for publication Jan. 14, 2020; published online Feb. 3, 2020.

1 Introduction

A longstanding challenge in optoelectronic materials is the experimental demonstration of high-performance p-type transparent conductive materials (p-TCMs), exhibiting properties on par with their n-type counterparts. Development of a p-TCM with broadband transparency and high conductivity that can be reliably applied in thin-film form would mark a significant breakthrough in the fields of transparent electronics, solar cells, and LEDs by enabling devices with reduced process complexity and minimum parasitic losses at the contacts.[1–3] Figure 1 shows example architectures that would benefit from the development of high-quality p-TCMs, including a silicon heterojunction solar cell,[4] a semitransparent halide perovskite solar cell or LED,[5,6] and a transparent complementary circuit built of p-type and n-type thin-film transistors (TFTs).[7,8]

The difficulty in experimentally realizing excellent p-TCMs lies in a contradiction of the fundamental requirements: p-type conductivity requires high hole mobility and low ionization potential to allow for p-type doping, but transparency requires a wide bandgap, which is most often found in metal oxides. The valence band maximum (VBM) of metal oxides is typically composed of highly localized oxygen 2p orbitals, which results in large hole effective masses and very low hole mobility. Furthermore, metal oxides are usually n-type with high ionization potential that hampers efforts on p-type doping. Cu-based delafossites and Cr-based oxides are some of the few oxides with experimentally reported p-type conductivity.[9,10] The first p-TCM,

*Address all correspondence to Monica Morales-Masis, E-mail: m.moralesmasis@utwente.nl

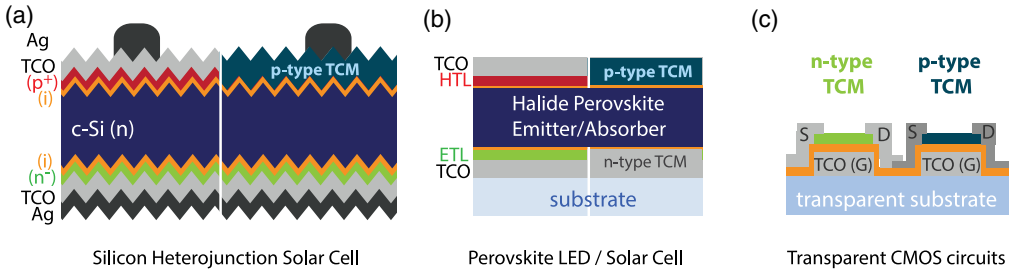

Fig. 1 Schematic diagrams of optoelectronic devices that will benefit from the development of p-type TCMs. (a) Silicon solar cells and (b) semitransparent halide perovskites solar cells or LEDs: a p-type TCM will allow to reduce parasitic absorption at the (front) contacts of the cell and could simplify processes such as the replacement of the hole selective contact and the TCO with one single layer; the p-type TCM providing hole selectivity and lateral transport. (c) Complementary electronics build of p- and n-type TFTs: p-type TCMs will allow the realization of full transparent electronics.

delafossite $CuAlO_2$ discovered in 1997, had a free hole carrier density of $N_h = 1.3 \times 10^{17}$ cm^{-3} and a hole mobility of $\approx$10 cm^2 V^{-1} s^{-1} resulting in a conductivity <1 S cm^{-1}.[11] Recently, Mg-doped $CuCrO_2$ was reported with a conductivity of 220 S cm^{-1}, representing the highest p-type conductivity reported to date.[12] However, this high p-type conductivity has thus far not been reproduced by other groups.[13] Moreover, even with 220 S cm^{-1}, the performance still falls short of standard n-type TCMs that routinely display conductivity >300 S cm^{-1}.[3,14]

With the advent of high-throughput computational screening and design approaches, numerous research articles proposing material compositions and structures with p-type conductivity and wide band gaps have been published. These predictions are based on coupling dispersion (delocalization) of the valence band (VB) with favorable defect formation chemistry in order to select materials with inherently high hole mobility and enhanced p-type dopability.[15–18] However, experimental realization of these materials currently lags behind theoretical predictions, creating an evident gap between computationally predicted disperse valence band materials (DVMs) and their experimental investigation. In this review, we present an overview of the experimental techniques and synthesis approaches reported on DVMs with the aim to bridge the gap between computational and experimental works on p-TCMs. The authors note that while oxide materials with promising p-type conductivity and transparency properties have received attention in the recent computational literature,[14,19] we focus herein on materials beyond oxides, as oxides are considered well-known chemistries with several synthesis approaches already at advanced stages of development.

2 Computational Screening for Disperse Valence Band Materials

VB dispersion as a design principle for p-TCMs has existed since the late 1990s.[11] Termed "chemical modification of the valence band," this strategy relies on orbital-mixing between Cu s-orbitals and O p-orbitals at the VBM to delocalize the VB and produce a shallow ionization potential thus facilitating p-type doping without self-compensation.[20] A growing number of computational works have extended this strategy by screening databases of inorganic materials for low hole effective mass (m_h^*) and p-type dopability, and using the resulting material set to deduce design principles for identifying candidate high-performance p-TCMs.[14,16,17]

Figure 2 gives a visual depiction of VB dispersion, including the relationship among VB dispersion (d^2E/dk^2), hole effective mass (m_h^*), and hole mobility (μ_h). A sharply curved VB has a large value of d^2E/dk^2 and hence a small m_h^* and large μ_h. For equal free hole carrier densities (N_h), the highest conductivity (σ_h) is achieved at highest (μ_h). Importantly, in Eq. (2) in Fig. 2, it is clear that μ_h depends on two variables: m_h^* and the scattering time (τ) (e is the fundamental electron charge). While the design principles here discussed are focused on lowering m_h^* to enhance μ_h, it is important to note that the crystal lattice and film microstructure will also play an important role in μ_h through τ. τ depends on the collisions of the conduction holes

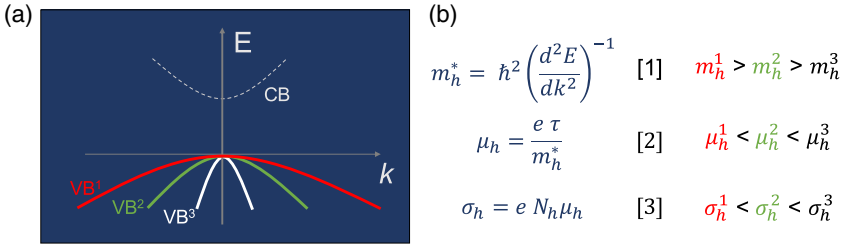

Fig. 2 (a) Schematic diagram depicting differing degrees of VB dispersion and an arbitrary conduction band. E represents the energy axis and k is the wave vector. VB_1 represents the least disperse (most localized) VB with the highest hole effective mass (m_h^1), whereas VB_3 represents the most disperse (least localized) VB with the lowest hole effective mass (m_h^3). This relationship is shown in writing in panel (b), where the hole effective mass of each is included in an inequality, along with expressions of hole effective mass (m_h^*), hole mobility (μ_h), and p-type conductivity (σ_h). The inverse proportionality between band dispersion (d^2E/dk^2) and hole effective mass as well as hole effective mass and hole mobility are represented in Eqs. (1) and (2), respectively.

(or conduction electrons in n-type materials) with lattice phonons (τ_{ph}), impurity atoms (τ_i), and grain boundaries or any other film imperfection (τ_{GB}). As the rates of these collisions are—to a good approximation—independent, the net relaxation time is given by: $1/\tau = 1/\tau_{ph} + 1/\tau_i + 1/\tau_{GB}$. More details regarding the scattering mechanisms are found in Ref. 21.

In particular, VB delocalization driven by anion-site chemistry was highlighted as leading to increased curvature (i.e., more disperse VBs) and thus low hole effective mass. One design principle identifies materials with mixed-anion chemistry, for example, oxy-chalcogenides or oxy-pnictides. In this case, the oxygen 2p-orbitals at the VBM are mixed with more disperse 3p-orbitals from the chalcogenide or pnictide anions, leading to better hole conductivity while maintaining transparency imparted by the oxide.[16] Another material class identified is binary nonoxide compounds.[15,18] These materials possess a VBM with significant contributions from anion p-states, which for nonoxide anions are more delocalized than the 2p orbitals of oxygen.[18] Materials such as sulfides, iodides, and especially phosphides[13,15,16,19,22] were found via high-throughput screening and first-principles calculations to commonly have $m_h^* < 5\ m_e$, with phosphides including many examples <1 m_e, owing to the metal-p and phosphorous-p orbital mixing at the VBM.[15]

Notable p-TCM candidates in these material classes are boron phosphide (BP),[15] copper iodide (CuI),[22–24] $CuAlS_2$,[25,26] (Zr,Hf)OS,[16,27] and Mg:LaCuOSe.[28] The band gap of BP can be up to 4 eV (direct)[15] with an indirect gap measured experimentally to be 2 eV.[29,30] CuI has a bandgap of 3.1 eV, a calculated hole effective mass of ~2 m_e, and native copper vacancy point defects that lead to degenerate p-type self-doping.[22,31,32] $CuAlS_2$ exhibits p-type conductivity >500 S cm^{-1} and a bandgap of 3.2 eV,[33] and Mg:LaCuOSe has a reported bandgap of 2.8 eV and hole effective mass of 1.6 m_e.[28] Despite these desirable properties, including some that are experimentally demonstrated, many challenges to experimental realization and/or widespread adoption of these materials exist, including difficulties in safely controlling precursors, such as sulfur and phosphorous, or avoiding secondary phases. The following sections are divided broadly into two material classes, nonoxides and oxychalcogenides, and subdivided further by specific compound. Experimental demonstrations of DVMs for p-TCM applications will be summarized and challenges particular to each chemistry will be discussed. Suggestions for overcoming these experimental roadblocks will be proposed, along with recommendations for future synthesis strategies and ultimate device integration.

3 Experimental Demonstrations

3.1 *Nonoxide Materials*

Two of the most widely studied nonoxide p-TCMs are BP and CuI. Experimental reports for BP extend back to 1957[34] and for CuI extend even further back to 1901.[35] P-type conduction was

measured in CuI as early as 1908, before the conception of positive-charge carriers was defined[36] whereas BP was not identified as p-type until 1960.[37] The first use of CuI as a p-type transparent layer in an optoelectronic device was published only in 2002,[38] and the first mention of it as a transparent conductor occurred in 2003.[39] For BP, the first mention of its potential as a p-type transparent conductor only occurred in 2017,[15] although previous works do report p-type character alone. As this review intends to focus on the experimental demonstrations and challenges of DVMs as p-type transparent conductors, the remaining discussion will focus solely on the more recent reports in which synthesis and characterization for p-TCM application was the main research goal.

3.1.1 *Copper iodide*

Application of CuI as a transparent hole-transport layer began in the dye-sensitized solar cell field,[38–40] and later continued in the fields of organic photovoltaics[41–48] and hybrid perovskite PV.[49] For a full review of the CuI literature, see Ref. 22. The first demonstration of p-type, transparent, and conducting CuI in thin-film form was vapor iodination of a Cu_2S precursor film.[50] Vapor iodination is one of the most common strategies for CuI thin-film synthesis, in addition to thermal evaporation.[51–53] The next most popular method is some variation of solution-coated synthesis, such as chemical bath deposition (CBD),[54] spin-coating,[55,56] or other similar strategies.[57] Vacuum deposition methods have been used, including pulsed-laser deposition[39,40,58–62] and reactive sputtering in iodine vapor,[63,64] but these techniques have received considerably less attention. In many cases, researchers simply purchase CuI powder and evaporate it onto glass substrates,[46,65–67] which highlights the ease of depositing CuI films. Such simplicity in synthesis has arguably led to the proliferation of CuI applications in optoelectronic devices over the years. This observation underlines an important point about experimental development of DVMs in general, namely that facile synthesis strategies are key to a given material's experimental success.

3.1.2 *Boron phosphide*

Contrary to the case of CuI, BP has only been applied as a p-type layer in an optoelectronic device in a few limited cases. The first mention of p-type BP in thin-film form was grown by chemical vapor deposition (CVD) using diborane and phosphine on a silicon substrate,[68] in which Schottky barrier diodes were prepared from p-BP/Al. Soon after, p-type BP applied in a photoelectrochemical cell for hydrogen evolution reaction.[69] Already at this stage, it was reported that BP could be doped either n-type or p-type, depending on the B : P ratio in the final material.[68–72] After these initial investigations into the electrical properties and p-type doping of BP, no reports of the p-type material occur until much later.[73–75]

Despite this absence of electrical characterization, many studies exist demonstrating BP synthesis by a variety of methods that include structural and optical characterization. One of the most common ways to make BP is through bulk synthesis techniques, such as flux growth or solid-state reaction.[30,76–79] Thin-film deposition of BP is almost invariably carried out by CVD of some kind, either metal-organic chemical vapor deposition (MOCVD),[73,80,81] or standard CVD,[68,70–72,74,75,82–85] or even plasma-enhanced CVD.[86] Other, less common deposition methods include vapor–liquid–solid growth,[87,88] thermal evaporation from powders in vacuum,[89] or sputtering in phosphine/Ar atmosphere.[90]

One observation from these experimental demonstrations is that the value of the direct bandgap of BP is still somewhat controversial. While some experimental reports indicate an indirect gap at 2 eV and a direct gap at 2.5 eV direct,[30] other work shows a direct gap as high as 6 eV,[37] and theoretical predictions indicate the direct gap could be 4 eV.[15] Experimental confirmation of the value of the direct bandgap in BP is one area where more research is needed going forward. In addition, while the level of p-type doping achievable in the literature (10^{17} to 10^{19} holes/cm^3)[68,73] supports the potential applicability of BP as a p-TCM, the overall dearth of electrical characterization for this material is another significant gap in the literature and represents an excellent opportunity for new experimental investigations.

3.1.3 *Copper aluminum sulfide*

Chalcopyrite copper aluminum sulfide ($CuAlS_2$) is another wide bandgap (~3.2 eV)[33,91] p-type material exhibiting a disperse VB that has been shown experimentally to have desirable electrical properties for TCM applications. Experimental demonstrations of this material have reported facile self-doping up to 10^{21} cm^{-3} coupled with a low hole effective mass estimated at 0.33 m_e, due to the hybridization of Cu 3d and S 3p orbitals at the VBM.[25] These features lead to high p-type conductivity in $CuAlS_2$ in the range of 250 to 540 S/cm.[25,33] Thin films of $CuAlS_2$ have been applied as a transparent p-type contacts in CIGS and organic solar cells,[33,92] but the material has otherwise received relatively limited attention in the literature. Despite the smaller number of studies, $CuAlS_2$ has been synthesized by a wide variety of deposition techniques, including solution-based techniques, such as CBD,[33,93] CVD methods, such as atomic layer deposition (ALD) and MOCVD,[91,92,94] solid-state synthesis routes,[25] thermal evaporation or sulfurization,[95–98] and even spray pyrolysis.[99,100] One important finding from these investigations is Cu-rich composition leading to higher conductivity,[26,33] due in part to the VB shifting upward with increasing copper content.[26] This decrease in ionization potential has been shown via first principles calculations to result in the Cu_{Al} acceptor transition level becoming more shallow, thus yielding lower ΔH_f and better doping efficiency.[26]

3.1.4 *Copper zinc sulfide*

Cu-alloyed zinc sulfide ($Cu_xZn_{1-x}S$), the final nonoxide material covered in this review, represents a special case, as it can be synthesized either as a heterostructural alloy[101] or as a nanocomposite of Cu_2S and ZnS, in which high conductivity stems from the Cu_2S phase and transparency is imparted by the wide bandgap of ZnS.[102] In the case of the alloy, p-type conductivity up to 40 S cm^{-1} and a bandgap of 3.1 eV have been reported.[103,104] For the nanocomposite, conductivity up 1000 S cm^{-1} has been shown in Refs. 102, 105, and 106 but at the cost of transparency with optical absorption onset lowering to 2.3 to 2.5 eV.[107,108] $Cu_xZn_{1-x}S$ can be deposited using vacuum methods such as pulsed layer deposition (PLD) and sputtering,[102,104,106] which provide the nonequilibrium growth conditions necessary to obtain the metastable heterostructural alloy. The nanocomposite can be also synthesized at ambient temperature via CBD[102,105,109,110] or by electrodeposition.[107,108,111] Of the nonoxide materials discussed, $Cu_xZn_{1-x}S$ has received the least experimental attention in the literature, perhaps due to challenges in controlling phase separation to achieve the desired properties as either a nanocomposite or alloy.

3.2 *Mixed-Anion Materials*

These material systems simultaneously contain an oxide (O^{2-}) and a chalcogenide (S^{2-}, Se^{2-}, and Te^{2-}) anion. Systems range from quinary compounds (e.g., doped, layered oxysulfides, such as Sr-doped LaCuOS) to simpler ternary compounds (e.g., ZrOS). Among experimentally realized p-TCMs, layered oxysulfides and oxyselenides are the most reported in the literature to date.

3.2.1 *Multinary oxy-chalcogenides*

The p-type conductivity of LaCuOS prepared by solid-state reaction was first demonstrated in 1991.[112] Earlier, the material was also prepared through oxidation of $LaCuS_2$ but only the crystal structure was reported.[113] It was not until the year 2000 that the combination of transparency (70% transmittance) and p-type conductivity (0.26 S cm^{-1}) was reported in the layered Sr-doped LaCuOS films prepared by radio-frequency sputtering.[114] The sputtering target was prepared as a composite of stoichiometrically mixed La_2S_3, Cu_2S, and La_2O_3 via solid-state reaction. Deposition was performed at 400°C, but crystallization was not achieved until a postannealing step at 800°C was applied.

Mg-doped LaCuOSe thin films were epitaxially grown by PLD.[28,115] Films were deposited on MgO (001) substrates from a $La_{0.8}Mg_{0.2}CuOSe$ ceramic target. A postannealing step at

1000°C was applied to crystallize the film. Very high hole carrier density was reported for this material, in the range of 10^{21}cm^{-3}; however, hole mobility was on the order of 3.4 cm^2/Vs and an effective mass of 1.6 ± 0.2 m_e (m_e is the rest mass of the electron) was estimated by the analysis of the free carrier absorption using the Drude model. A band gap of 2.8 eV was reported; however, the films presented high absorbance in the visible range of the spectra (estimated 50% transmission at 600 nm wavelength). After this report, hybrid density functional theory was used to suggest alternative p-type dopants for LaCuOSe.[116] Sr^{2+} or Ca^{2+} was identified as optimal acceptor dopants instead of the previously reported Mg^{2+}. Experimental validation of these acceptors has not yet been reported following this computational work.

Finally, the layered oxysulfide $[Cu_2S][Sr_3Sc_2O_5]$ was synthesized (only in bulk form) and reported to have a hole mobility of 150 cm^2/Vs. However, p-type carrier density was low (order of 10^{17} cm^{-3}) resulting in a conductivity of only 2.8 S/cm.[117] While the mobility was very promising, no report of thin-film synthesis of this material has been reported to date.

3.2.2 *Ternary oxy-chalcogenides*

P-type Y-doped ZrOS nanocrystals were synthesized by high-temperature solid-state reaction.[27] The design principle consisted of synthesizing tetragonal ZrOS (t-ZrOS), as calculations indicated that the S $3p_{x/y}$ orbitals form a shallower and sharper VBM (both requirements for p-type dopability and high hole mobility) compared to cubic ZrOS (c-ZrOS), although the bandgap of the cubic phase was predicted to be significantly wider. Hole effective masses of 0.24 m_e and 0.37 m_e were calculated for t-ZrOS and c-ZrOS, respectively. Conductivity of 10^{-2} S/cm was determined by Seebeck coefficient measurement; however, no Hall effect measurements were reported as reliable measurements require the fabrication of thin films. It is therefore the fabrication of thin films and their optical and transport property measurements that will confirm the potential of this material.

Thin films of HfOS have not been reported in literature to our knowledge, but interestingly, it has been demonstrated that controlling the oxygen vacancies in HfO_{2-x} results in a formation of a semimetal with p-type conductivity.[118] Hole carrier density on the order of 10^{21} cm^{-3} was reported for films fabricated with molecular beam epitaxy, yet the band gap was too low for TCM applications (~1 eV).[118] Moreover, in 2013, first principles calculations were used to propose tetragonal Hf_2O_3 and Zr_2O_3 as semimetals with high hole carrier density as well.[119] These reports and others focused strictly on depositing the related oxides could serve as inspiration for demonstrating thin-film HfOS and ZrOS using similar approaches.

Tin oxyselenide (SnOSe) thin films with p-type conductivity have recently been reported in the experimental literature.[120] Thin films were prepared by reactive co-sputtering from Sn and SnSe targets under oxygen atmosphere (substrate temperature not reported). After deposition, the films were annealed at 300°C under vacuum. Annealed films with the composition $SnSe_{0.56}O_{0.44}$ exhibited hole mobility of 15 cm^2/Vs and hole carrier density of 1.2×10^{17}cm^{-3}. The band gap (1.93 eV) is however too low to become a state of the art p-TCM. Experimental efforts would need to focus on developing strategies to increase doping and widen the band gap in order to further assess the usefulness of this material system for p-TCM applications.

Table 1 summarizes selected properties of the DVMs covered herein, separated by whether or not the materials have been experimentally demonstrated in the literature. We caution the reader that conductivity values must always be weighed against transparency, as not every material with high conductivity in Table 1 exhibits high transparency (e.g., BP). A good indication for transparency in the visible range is the band gap (i.e., Eg $>$ 3 eV). However, several of the reported Eg in the table are from computational studies, and therefore not conclusive in terms of "real" electrode performance. Successful synthesis methods for each material are also listed, which is a key aspect of this review. One aim of the discussion in this work is to assess whether particular synthesis methods, chemistries, or other features tend to facilitate experimental demonstration of DVMs. Looking at Table 1, it is clear that no one particular synthesis method wins. Instead, chemical complexity appears to be the more important factor in deciding whether a given material has received extensive experimental attention in the literature or not.

Table 1 Summary of properties and synthesis methods for DVMs.

Material	Hole effective mass	Bandgap (eV)	Demonstrated? (Y/N)	Mobility (cm^2/Vs)	Conductivity (S/cm)	Deposition Method(s)
CuI	0.3 (lh) 2.14 to 2.4 (hh)[31,32]	3.1[22]	Y	6, 43.9[121,122]	0.3 to 94.3[36,121–124]	Iodination of thin film, PLD, solid-state synthesis, solution-processing, sputtering, thermal evaporation
BP	0.35[15]	2.0 (ind), 2.5 to 4.0 (dir), 6.0 (dir)[15,30,37]	Y	1.77, 70[73,125]	0.67 to 707[37,73,125,126]	CVD, MOCVD, PECVD, solid-state synthesis, sputtering, thermal evaporation, vapor–liquid–solid
Cu-Zn-S	—	2.3 to 3.8[102,107–109,111]	Y	1.0 to 1.4, 0.5 to 1.6[102,106]	42, 54, 752[102,104,106]	CBD, PLD, sputtering
$CuAlS_2$	0.33[25]	2.88 to 3.4[25,33,91]	Y	1.52, 21.2[25,33]	250, 546[25,33]	ALD, CBD, MOCVD, solid-state synthesis, spray pyrolysis, sulfurization of metal, thermal evaporation
LaCuOS	1[127]	3	Y	—	0.012[114]	Solid-state synthesis, sputtering
$La_{0.95}Sr_{0.05}CuOS$	—	—	Y	—	0.26[114]	Solid-state synthesis, sputtering
Mg:LaCuOSe	1.6 ± 0.2[28]	2.8[28]	Y	3.4[28]	950[28]	PLD with postannealing
$[Cu_2S][Sr_3Sc_2O_5]$	—	3.1[117]	Y	150[117]	2.8[117]	Solid-state synthesis
ZrOS (tetragonal)	0.24[27]	2.5 (dir. forbidden)[27]	Y	—	0.01[27]	Solid-state synthesis
SnOSe	0.6 to 1.99[120]	1.93[120]	Y	15[120]	0.29[120]	Sputtering
Computationally identified only						
ZrOS (cubic)	0.37[27]	4.25 (ind)[16]	N	—	—	—
HfOS	1.25[16]	4.5	N	—	—	—
La_2SeO_2	0.92[128]	3.49	N	—	—	—

4 Experimental Challenges

4.1 *Nonoxide Materials*

4.1.1 *Copper iodide*

The experimental challenges faced by CuI are not in the synthesis itself, which, as shown above, is straightforward and can be carried out by a number of methods. On the contrary, the main challenges are in the properties of the layer after deposition. Air and moisture stability of is a well-documented issue,[51,129] due at least in part to the low migration energy barrier for Cu, especially at temperatures above 200°C.[130–132] Another problem relevant to its application as a transparent conductor is high surface roughness when synthesized using the common method of vapor iodination of Cu films or by PLD,[52,58,121] which reduces the transparency significantly. However, thermal evaporation[133,134] and sputtering techniques[63,64] do successfully address the surface roughness problem, in addition to vapor iodination using a compound precursor film, such as Cu_3N or Cu_2S.[52,135] Despite these challenges, CuI is one of the most widely studied DVMs in the literature today, owing to a few factors, one important factor being the ease with which the material can be synthesized in phase-pure form. Indeed, the absence of competing secondary phases and the propensity to self-dope are two features of CuI that continue to facilitate its investigation and application in the literature.

4.1.2 *Boron phosphide*

In the case of BP, the biggest experimental challenge is the highly inert nature of elemental boron,[78] which has led researchers to rely on deposition techniques that utilize more reactive forms of boron—specifically, diborane (B_2H_2) in CVD-based processes. The drawback to this approach is the high toxicity of both diborane and phosphine,[86] which require special safety measures for use. Toxicity of phosphine is also an obstacle for attempts at sputtering BP,[90] which increases the reactivity of boron via plasma-based deposition but thus far has utilized a gas-phase phosphorous source. One possible alternative could be a solid phosphorous source for evaporation in vacuum in conjunction with a boron sputtering target, although careful management of side reactions with phosphorous and water or air would still need to be undertaken.

Keeping the above concerns in mind, it is still the case that successful thin-film deposition of BP has been demonstrated in the literature for years. What is lacking in the literature are studies focused on electrical characterization of p-type BP. Given that several reports of p-type conductivity already exist,[68,71,73–75] and that this material has been computationally identified as having a disperse VB suitable for high mobility of holes,[15] all that remains is to couple known deposition recipes with standard electrical characterization techniques to experimentally confirm the computational predictions.

4.1.3 *Sulfides*

As with any sulfide, experimental challenges to synthesizing $CuAlS_2$ or Cu-alloyed ZnS thin films arise mostly related to sulfur management, in particular the need to avoid toxicity from hydrogen sulfide (H_2S). This is the case in any vacuum-based method, CVD-based deposition, or thermal evaporation, as precursors used to deliver sulfur to the growing film typically lead to unintentional formation (or incomplete utilization) of H_2S.[91,92] For this reason, solution-based methods are more attractive since sulfur-containing reagents can be more readily controlled. However, CBD can lead to inhomogeneity in the resulting film,[33] and often such films require postdeposition annealing to obtain good crystallinity and the desired TCM properties, which leads again to the issues of sulfur management. However, the challenges presented by solution synthesis may be easier to overcome by a wider range of researchers than those presented by CVD methods, given that less infrastructure is required to properly trap or ventilate sulfur-containing by-products of an anneal than in the case of direct H_2S delivery to a deposition chamber.

4.2 *Mixed-Anion Materials*

Some of the challenges of growing mixed-anion materials lie in the different formation energies for oxides versus chalcogenides and in the metastability of some phases, resulting in phase segregation. Therefore, synthesis approaches promoting chemical stabilization should be preferred. In literature, solid-state synthesis has been the most common technique used for making oxychalcogenide bulk crystals.[136] But this technique requires high thermal budgets, is a lengthy process, and is not well-suited to optoelectronic device integration. However, reported recipes can be applied for the fabrication of sputtering or PLD targets, through powder milling and pressing. Once a target is created, a single-source deposition should be possible with these techniques.

For the formation of mixed-anion thin films, PVD (evaporation, sputtering, and PLD), and CVD (ALD and MOCVD) offer several advantages, including their compatibility with device fabrication. Differing volatility or sputtering rates of the various species in mixed-anion materials can lead to challenges in single-source deposition. To overcome such challenges, multisource deposition can be applied, such as thermal coevaporation or cosputtering. Multistep processes can also be an effective synthesis strategy in making multinary oxychalcogenides, such as LaCuOS,[114] in which initial deposition is followed by postdeposition annealing in reactive or nonreactive atmospheres and allows control of the phases formed at each processing step.[137,138] In the case of oxychalcogenides, controlled oxidation could be a third synthesis step. It is important to note that the order sulfurization (selenization) + oxidation or oxidation + sulfurization (selenization) should be determined based on the formation energy and binding energy of the competing binary phases. For example, to fabricate ZrOS films using a multistep process, formation of ZrS_x must be undertaken first (in an oxygen-free atmosphere), as the formation energy of ZrO_2 is much lower than that of ZrS_2 (by $\sim$1.8eV).[139] Once a sulfide phase is formed, oxidation can then be performed by, for example, annealing in controlled oxygen atmosphere as well as heating at a controlled rate to avoid the segregation of ZrO_x and ZrS_x phases. The same recommendations apply for HfOS. Cosputtering from compound targets, such as ZrS_2 and ZrO_2 for ZrOS or HfS_2 and HfO_2 sources for HfOS, is another promising method for synthesizing the ternary phases without segregation of binary compounds.

ALD and PLD are also promising techniques for these oxychalcogenide compounds. ALD allows the alternating introduction of precursors, such as H_2S, water, and metal–organic precursor gases, and gives atomic-level control to build these compounds element by element.[140] PLD on the other hand has the advantage that the use of a high energy laser allows nonequilibrium ablation of a target (containing all the required elements of the multicomponent film) and therefore stoichiometric transfer is possible independent of the volatility of the components.[141] It is important to note that PLD has commonly been used for epitaxial growth of films at high temperature. However, PLD has a great potential for nonepitaxial low-temperature fabrication of thin films, due to the possibility of enabling single-source deposition of multicomponent materials.

Up to now, we have only discussed vacuum-based deposition techniques for mixed-anion materials. Beyond vacuum-based processes, solution processing, such as single-step hydrothermal synthesis and two-step CBD, has proven successful to access selenide and oxy-selenide phases at low temperatures.[142] The accessibility of these approaches makes them worth exploring as well, in order to evaluate the feasibility of using low-cost solution synthesis for integration of oxy-chalcogenide p-TCM materials in optoelectronic devices.

5 Summary and Outlook

One general similarity among the DVMs discussed herein that have been experimentally demonstrated as a thin film is that each could be deposited by a variety of techniques, ranging from vacuum-based deposition to solution-coating. In each case, the nonoxide anion (sulfide, selenide, phosphide, or iodide) presents challenges to safe delivery during film growth that are not similarly present when dealing with oxides. These challenges must be handled differently depending on the deposition technique chosen, but no particular method of thin-film synthesis is consistently superior, so long as sufficient resources are dedicated to developing a finely

controlled process. Researchers interested in investigating one of the nonoxides or oxychalcogenides discussed in this review can apparently take their pick of deposition methods for which their lab is best equipped, given the sheer number of different techniques represented in the literature thus far. Overall, the important point is to recognize that thin-film synthesis is critically enabling for electrical characterization and ultimate device integration for candidate p-TCMs and should be the focus of experimental efforts going forward.

Looking more closely at publication trends among the nonoxide and oxychalcogenide materials, a few more observations can be made. The total number of publications for each material decreases going from CuI to BP to $CuAlS_2$ and finally to Cu-Zn-S and the oxychalcogenides. One observation is that the two materials with the most publications are both binary compounds, whereas the ternary and multinary materials have received significantly less research attention. A possible explanation for this is the relatively simpler phase space of binary compounds compared to multinary materials, which facilitates synthesis and characterization. Another observation is that materials, such as Cu-Zn-S and $[Cu_2S][Sr_3Sc_2O_5]$, are known to exhibit Cu_2S phase segregation, which renders them more difficult to accurately characterize, despite the fact that the nanocomposite of Cu-Zn-S in particular has been shown to exhibit desirable TCM properties. In general, these observations suggest that focusing research attention on binary and ternary materials with fewer (or less favorable to form) secondary phases, as opposed to the more-complicated quaternary and quinary compounds, is a prudent investigative strategy to bridge the p-TCMs gap.

Moreover, we propose that computational screening and first principles predictions of p-TCMs attempt to translate chemical potential diagrams into practical experimental considerations such as partial pressures or material fluxes in a reaction chamber. An example of such translation can be seen for La_2SeO_2 in Refs. 116 and 128. For the experimentalist, it is important to build a good understanding between reported chemical potentials at which phases are stable, and partial pressures during the growth of the phases.

One final point is the absence of experimental confirmations of predicted properties for many of the materials discussed herein. For materials such as BP, reports of electrical properties are scarce, and the absence of thin film examples for some multinary oxychalcogenides has thus far precluded typical characterization campaigns for transparency and conductivity. Another important characterization that is within reach for experimentalists today is visualizing VB

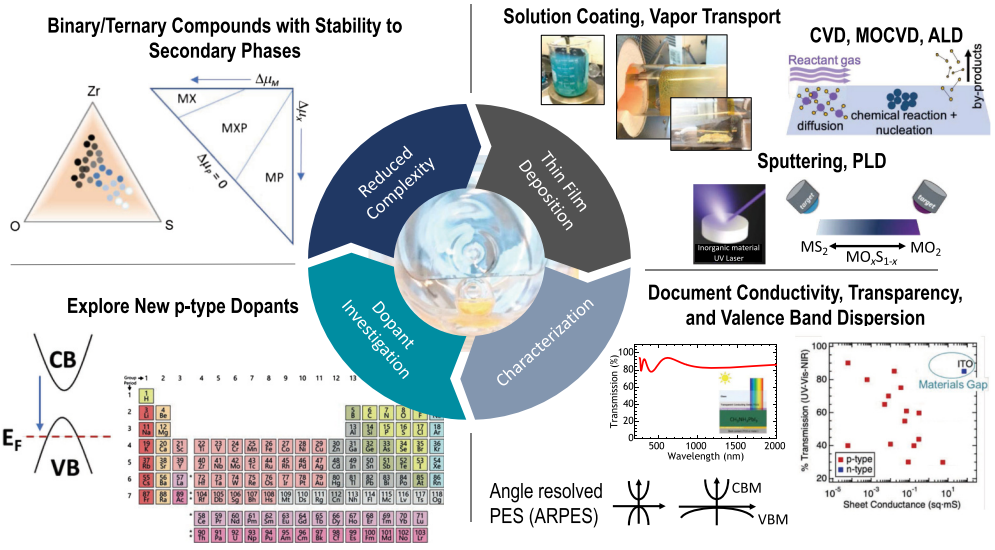

Fig. 3 Summary of the four recommendations for bridging the experimental literature gap in p-TCMs. Materials with reduced chemical complexity deposited in thin-film form should be the focus of experimental research efforts going forward. Investigating new candidates for p-type dopants in previously synthesized materials and working to document conductivity, transparency, and VB dispersion for computationally predicted materials are all fruitful research paths for the p-TCM community.

dispersion using techniques such as angle-resolved photoemission spectroscopy. Applying this measurement to predicted DVMs to assess the curvature of the VB as composition changes for a given material (especially those with clear binary endpoints, such as $CuAlS_2$ and ZrOS) would be a fascinating and informative research thrust. A summary of the recommendations distilled from this review is depicted graphically in Fig. 3. Ultimately, it will be shared knowledge between computational materials science and thin film synthesis supported by state-of-the-art characterization techniques that will allow us to correlate experiment with predictions and finally close the p-TCMs gap and integrate the best material into optoelectronic devices for maximum impact.

Acknowledgments

A.N.F. acknowledges funding from the European Union's Horizon 2020 Marie Skłodowska-Curie Actions under Grant Agreement No. 792720 (CLAReTE). M.M.M. acknowledges financial support from the NWO Start Up Grant 2019, Grant No. STU.019.026 (BRIDGE). The authors declare no conflicts of interest.

References

1. D. S. Ginley and J. D. Perkins, "Transparent conductors," in *Handbook of Transparent Conductors*, D. S. Ginley, Ed., pp. 1–25, Springer, Boston, Massachusetts (2011).
2. H. Hosono, "Exploring electro-active functionality of transparent oxide materials," *Jpn. J. Appl. Phys.* **52**(9), 090001 (2013).
3. M. Morales-Masis et al., "Transparent electrodes for efficient optoelectronics," *Adv. Electron. Mater.* **3**(5), 1600529 (2017).
4. C. Battaglia, A. Cuevas, and S. De Wolf, "High-efficiency crystalline silicon solar cells: status and perspectives," *Energy Environ. Sci.* **9**(5), 1552–1576 (2016).
5. B. R. Sutherland and E. H. Sargent, "Perovskite photonic sources," *Nat. Photonics* **10**(5), 295–302 (2016).
6. J.-P. Correa-Baena et al., "Promises and challenges of perovskite solar cells," *Science* **358**(6364), 739–744 (2017).
7. A. Daus et al., "Flexible CMOS electronics based on p-type $Ge_2Sb_2Te_5$ and n-type $InGaZnO_4$ semiconductors," in *IEEE Int. Electron Devices Meeting*, pp. 8.1.1–8.1.4 (2017).
8. K. Nomura, T. Kamiya, and H. Hosono, "Ambipolar oxide thin-film transistor," *Adv. Mater.* **23**(30), 3431–3434 (2011).
9. H. Hosono, "Recent progress in transparent oxide semiconductors: materials and device application," *Thin Solid Films* **515**(15), 6000–6014 (2007).
10. H. Kawazoe et al., "Transparent p-type conducting oxides: design and fabrication of p-n heterojunctions," *MRS Bull.* **25**(8), 28–36 (2000).
11. H. Kawazoe et al., "P-type electrical conduction in transparent thin films of $CuAlO_2$," *Nature* **389**(6654), 939–942 (1997).
12. R. Nagarajan et al., "p-type conductivity in $CuCr_{1-x}Mg_xO_2$ films and powders," *J. Appl. Phys.* **89**(12), 8022–8025 (2001).
13. L. Farrell et al., "Synthesis of nanocrystalline Cu deficient $CuCrO_2$: a high figure of merit p-type transparent semiconductor," *J. Mater. Chem. C* **4**(1), 126–134 (2016).
14. G. Brunin et al., "Transparent conducting materials discovery using high-throughput computing," *npj Comput. Mater.* **5**(1), 1–13 (2019).
15. J. B. Varley et al., "High-throughput design of non-oxide p-type transparent conducting materials: data mining, search strategy, and identification of boron phosphide," *Chem. Mater.* **29**(6), 2568–2573 (2017).
16. G. Hautier et al., "Identification and design principles of low hole effective mass p-type transparent conducting oxides," *Nat. Commun.* **4**, 2292 (2013).
17. B. A. D. Williamson et al., "Engineering valence band dispersion for high mobility p-type semiconductors," *Chem. Mater.* **29**(6), 2402–2413 (2017).

18. R. K. M. Raghupathy et al., "Rational design of transparent p-type conducting non-oxide materials from high-throughput calculations," *J. Mater. Chem. C* **6**(3), 541–549 (2018).
19. M. Graužinytė, S. Goedecker, and J. A. Flores-Livas, "Towards bipolar tin monoxide: revealing unexplored dopants," *Phys. Rev. Mater.* **2**(10), 104604 (2018).
20. A. Zunger, "Practical doping principles," *Appl. Phys. Lett.* **83**(1), 57–59 (2003).
21. K. Ellmer, "Past achievements and future challenges in the development of optically transparent electrodes," *Nat. Photonics* **6**(12), 809–817 (2012).
22. M. Grundmann et al., "Cuprous iodide: a p-type transparent semiconductor, history, and novel applications," *Phys. Status Solidi A* **210**, 1671–1703 (2013).
23. H. Hernández-Cocoletzi et al., "Density functional study of the structural properties of copper iodide: LDA vs. GGA calculations," *J. Nano Res.* **5**(1), 25–30 (2009).
24. T. Jun et al., "Material design of p-type transparent amorphous semiconductor, Cu-Sn-I," *Adv. Mater.* **30**(12), 1706573 (2018).
25. F. Q. Huang, M. L. Liu, and C. Yang, "Highly enhanced p-type electrical conduction in wide band gap $Cu1_xAl_{1-x}S_2$ polycrystals," *Sol. Energy Mater. Sol. Cells* **95**(10), 2924–2927 (2011).
26. D. Huang et al., "Understanding the high p-type conductivity in Cu-excess $CuAlS_2$: a first-principles study," *Appl. Phys. Express* **9**(3), 031202 (2016).
27. T. Arai et al., "Chemical design and example of transparent bipolar semiconductors," *J. Am. Chem. Soc.* **139**(47), 17175–17180 (2017).
28. H. Hiramatsu et al., "Heavy hole doping of epitaxial thin films of a wide gap p-type semiconductor, LaCuOSe, and analysis of the effective mass," *Appl. Phys. Lett.* **91**(1), 012104 (2007).
29. A. Agui, S. Shin, and Y. Kumashiro, "Electronic structure of BP studied by resonant soft x-ray emission spectroscopy," *J. Phys. Soc. Jpn.* **68**(1), 166–169 (1999).
30. Y. A. Nikolaev et al., "Photosensitive structures based on boron phosphide single crystals," *Semiconductors* **37**(8), 923–926 (2003).
31. J. Wang, J. Li, and S.-S. Li, "Native p-type transparent conductive CuI via intrinsic defects," *J. Appl. Phys.* **110**(5), 054907 (2011).
32. B. Hönerlage, C. Klingshirn, and J. B. Grun, "Spontaneous emission due to exciton—electron scattering in semiconductors," *Phys. Status Solidi B* **78**(2), 599–608 (1976).
33. X. Dai et al., "A simple synthesis of transparent and highly conducting p-type $Cu_xAl_{1-x}S_y$ nanocomposite thin films as the hole transporting layer for organic solar cells," *RSC Adv.* **8**, 16887–16896 (2018).
34. P. Popper and T. A. Ingles, "Boron phosphide, a III-V compound of zinc-blende structure," *Nature* **179**(4569), 1075 (1957).
35. W. Spring, "Über das spezifische Gewicht des Kupferjodürs," *Z. Anorg. Chem.* **27**(1), 308–309 (1901).
36. K. Bädeker, "Über die elektrische Leitfähigkeit und die thermoelektrische Kraft einiger Schwermetallverbindungen," *Ann. Phys.* **327**(4), 749–766 (1907).
37. B. Stone and D. Hill, "Semiconducting properties of cubic boron phosphide," *Phys. Rev. Lett.* **4**(6), 282–284 (1960).
38. A. Konno et al., "Effect of imidazolium salts on the performance of solid-state dyesensitized photovoltaic cell using copper iodide as a hole collector," *Electrochemistry* **70**(6), 432–434 (2002).
39. M. Rusop et al., "Properties of pulsed-laser-deposited cui and characteristics of constructed dye-sensitized TiO_2|Dye|CuI solid-state photovoltaic solar cells," *Jpn. J. Appl. Phys.* **42**(8), 4966–4972 (2003).
40. M. Rusop et al., "Copper iodide thin films as a p-type electrical conductivity in dye-sensitized p-CuI|Dye|n-TiO_2 heterojunction solid state solar cells," *Surf. Rev. Lett.* **11**(6), 577–583 (2004).
41. Y. Zhou et al., "Glancing angle deposition of copper iodide nanocrystals for efficient organic photovoltaics," *Nano Lett.* **12**(8), 4146–4152 (2012).
42. J. W. Kim et al., "High performance organic planar heterojunction solar cells by controlling the molecular orientation," *Curr. Appl. Phys.* **13**(1), 7–11 (2013).

43. J. C. Bernede et al., "MoO_3/CuI hybrid buffer layer for the optimization of organic solar cells based on a donor-acceptor triphenylamine," *Sol. Energy Mater. Sol. Cells* **110**, 107–114 (2013).
44. J. A. Christians, R. C. M. Fung, and P. V. Kamat, "An inorganic hole conductor for organo-lead halide perovskite solar cells. Improved hole conductivity with copper iodide," *J. Am. Chem. Soc.* **136**(2), 758–764 (2014).
45. W. Sun et al., "Solution-processed copper iodide as an inexpensive and effective anode buffer layer for polymer solar cells," *J. Phys. Chem. C* **118**(30), 16806–16812 (2014).
46. V. V. Travkin et al., "A hybrid CuI/fullerene heterojunction in transparent flexible photovoltaic cells," *Fullerenes Nanotubes Carbon Nanostruct.* **23**(8), 721–724 (2015).
47. K. Zhao et al., "Highly efficient organic solar cells based on a robust room-temperature solution-processed copper iodide hole transporter," *Nano Energy* **16**, 458–469 (2015).
48. S. A. Mohamed et al., "CuI as versatile hole-selective contact for organic solar cell based on anthracene-containing PPE-PPV," *Sol. Energy Mater. Sol. Cells* **143**, 369–374 (2015).
49. B. Gil et al., "Recent progress in inorganic hole transport materials for efficient and stable perovskite solar cells," *Electron. Mater. Lett.* **15**(5), 505–524 (2019).
50. T. K. Chaudhuri et al., "A chemical method for preparing copper iodide thin films," *Jpn. J. Appl. Phys.* **29**(2), L352–L354 (1990).
51. V. Raj et al., "Introduction of TiO_2 in CuI for its improved performance as a p-type transparent conductor," *ACS Appl. Mater. Interfaces* **11**(27), 24254–24263 (2019).
52. N. Yamada et al., "High-mobility transparent p-type CuI semiconducting layers fabricated on flexible plastic sheets: toward flexible transparent electronics," *Adv. Electron. Mater.* **3**(12), 1700298 (2017).
53. K. Tennakone et al., "Preparation of thin polycrystalline films of cuprous iodide and photoelectrochemical dye-sensitization," *Thin Solid Films* **217**(1–2), 129–132 (1992).
54. R. N. Bulakhe et al., "Deposition of copper iodide thin films by chemical bath deposition (CBD) and successive ionic layer adsorption and reaction (SILAR) methods," *Curr. Appl. Phys.* **13**(8), 1661–1667 (2013).
55. M. Rahman et al., "Unraveling the electrical properties of solution-processed copper iodide thin films for CuI/n-Si solar cells," *Mater. Res. Bull.* **118**, 110518 (2019).
56. A. Liu et al., "Room-temperature solution-synthesized p-type copper(I) iodide semiconductors for transparent thin-film transistors and complementary electronics," *Adv. Mater.* **30**(34), 1802379 (2018).
57. K. Tennakone et al., "Deposition of thin conducting films of CuI on glass," *Sol. Energy Mater. Sol. Cells* **55**(3), 283–289 (1998).
58. P. M. Sirimanne et al., "Characterization of transparent conducting CuI thin films prepared by pulsed laser deposition technique," *Chem. Phys. Lett.* **366**(5–6), 485–489 (2002).
59. M. Rusop et al., "Annealing temperature effects on synthesis of n-TiO_2/dye/p-CuI solid-state solar cells," *Jpn. J. Appl. Phys.* **44**(4B), 2560–2567 (2005).
60. M. Rusop et al., "Optical band gap excitation and photoelectron generation in titanium dioxide-based solid state solar cells," *Surf. Rev. Lett.* **12**(5–6), 681–689 (2005).
61. M. Rusop et al., "Study on the properties and charge generation in dye-sensitized n-TiO_2/dye/p-CuI solid state photovoltaic solar cells," *Appl. Surf. Sci.* **252**(20), 7389–7396 (2006).
62. B. L. Zhu and X. Z. Zhao, "Transparent conductive CuI thin films prepared by pulsed laser deposition," *Phys. Status Solidi A* **208**(1), 91–96 (2011).
63. T. Tanaka, K. Kawabata, and M. Hirose, "Transparent, conductive CuI films prepared by rf-dc coupled magnetron sputtering," *Thin Solid Films* **281–282**, 179–181 (1996).
64. C. Yang et al., "Room-temperature synthesized copper iodide thin film as degenerate p-type transparent conductor with a boosted figure of merit," *Proc. Natl. Acad. Sci. U. S. A.* **113**(46), 12929–12933 (2016).
65. P. Y. Stakhira and V. V. Cherpak, "The properties of heterojunction based on CuI/pentacene/Al," *Vacuum* **83**(8), 1129–1131 (2009).
66. P. Stakhira et al., "Characteristics of organic light emitting diodes with copper iodide as injection layer," *Thin Solid Films* **518**(23), 7016–7018 (2010).

67. D. K. Kaushik et al., "Thermal evaporated copper iodide (CuI) thin films: a note on the disorder evaluated through the temperature dependent electrical properties," *Sol. Energy Mater. Sol. Cells* **165**, 52–58 (2017).
68. Y. Kumashiro and Y. Okada, "Schottky barrier diodes using thick, well-characterized boron phosphide wafers," *Appl. Phys. Lett.* **47**(1), 64–66 (1985).
69. J. Lee et al., "Photoelectrochemical behavior of p-type boron phosphide photoelectrode in acidic solution," *Bull. Chem. Soc. Jpn.* **58**(9), 2634–2637 (1985).
70. A. Goossens, E. M. Kelder, and J. Schoonman, "Polycrystalline boron phosphide semiconductor electrodes," *Ber. Bunsengesellschaft Phys. Chem.* **93**(10), 1109–1114 (1989).
71. Y. Kumashiro, M. Hirabayashi, and S. Takagi, "Boron phosphide as a refractory semiconductor," *MRS Proc.* **162**, 585–594 (1989).
72. A. Goossens et al., "Structural, optical, and electronic properties of silicon/boron phosphide heterojunction photoelectrodes," *Ber. Bunsengesellschaft Phys. Chem.* **95**(4), 503–510 (1991).
73. T. Udagawa and G. Shimaoka, "Heteroepitaxial growth of boronphosphide III–V semiconductor on silicon by organometallic chemical vapor deposition," *J. Ceram. Process. Res.* **4**(2), 80–83 (2003).
74. B. Padavala et al., "Cubic boron phosphide epitaxy on zirconium diboride," *J. Cryst. Growth* **483**, 115–120 (2018).
75. N. Ding et al., "Controllable carrier type in boron phosphide nanowires toward homostructural optoelectronic devices," *ACS Appl. Mater. Interfaces* **10**(12), 10296–10303 (2018).
76. X. Feng et al., "Low temperature synthesis of boron phosphide nanocrystals," *Mater. Lett.* **59**(8–9), 865–867 (2005).
77. V. A. Mukhanov et al., "Self-propagating high-temperature synthesis of boron phosphide," *J. Superhard Mater.* **35**(6), 415–417 (2013).
78. K. Woo, K. Lee, and K. Kovnir, "BP: synthesis and properties of boron phosphide," *Mater. Res. Express* **3**(7), 074003 (2016).
79. L. Shi et al., "n-type boron phosphide as a highly stable, metal-free, visible-light active photocatalyst for hydrogen evolution," *Nano Energy* **28**, 158–163 (2016).
80. M. Odawara et al., "Suppression of indium vaporization from GaN/GaInN superlattice by BP capping layer," *J. Cryst. Growth* **263**(1–4), 645–647 (2004).
81. M. Odawara, T. Udagawa, and G. Shimaoka, "Organometallic chemical vapor deposition growth of heterostructure of wide band gap and transparent boron phosphide on silicon," *Jpn. J. Appl. Phys.* **44**(1B), 681–683 (2005).
82. A. Goossens and J. Schoonman, "An impedance study of boron phosphide semiconductor electrodes," *J. Electrochem. Soc.* **139**(3), 893–900 (1992).
83. B. Padavala et al., "Epitaxy of boron phosphide on aluminum nitride(0001)/sapphire substrate," *Cryst. Growth Des.* **16**(2), 981–987 (2016).
84. B. Padavala et al., "CVD growth and properties of boron phosphide on 3C-SiC," *J. Cryst. Growth* **449**, 15–21 (2016).
85. S. P. Huber et al., "Exploiting the P L2,3 absorption edge for optics: spectroscopic and structural characterization of cubic boron phosphide thin films," *Opt. Mater. Express* **6**(12), 3946 (2016).
86. W. Liu et al., "Structural, mechanical properties and composition analysis of boron phosphide coatings," *J. Alloys Compd.* **538**, 169–172 (2012).
87. E. Schroten, A. Goossens, and J. Schoonman, "Synthesis of nanometer-scale boron phosphide whiskers by vapor-liquid-solid chemical vapor deposition," *J. Appl. Phys.* **79**(8), 4465–4467 (1996).
88. E. Schroten, A. Goossens, and J. Schoonman, "Large-surface-area boron phosphide liquid junction solar cells," *J. Electrochem. Soc.* **146**(6), 2045–2048 (1999).
89. S. Dalui et al., "Boron phosphide films prepared by co-evaporation technique: synthesis and characterization," *Thin Solid Films* **516**(15), 4958–4965 (2008).
90. Z. C. Jia et al., "Effect of gas flow ratio on the microstructure and mechanical properties of boron phosphide films prepared by reactive magnetron sputtering," *Appl. Surf. Sci.* **258**(1), 356–360 (2011).

91. J. Damisa et al., "Morphological and optical study of thin films of $CuAlS_2$ deposited by metal organic chemical vapour deposition technique," *Mater. Res. Express* **4**(8), 086412 (2017).
92. N. Schneider et al., "Transparent ohmic contact for CIGS solar cells based on p-type aluminum copper sulfide material synthesized by atomic layer deposition," *ACS Appl. Energy Mater.* **1**(12), 7220–7229 (2018).
93. D. N. Okoli, A. J. Ekpunobi, and C. E. Okeke, "Optical properties of chemical bath deposited $CuAlS_2$ thin films," *Pac. J. Sci. Technol.* **7**(1) (2006).
94. L. Duclaux et al., "Simulation and growing study of Cu-Al-S thin films deposited by atomic layer deposition," *Thin Solid Films* **594**, 232–237 (2015).
95. A. U. Moreh, M. Momoh, and B. Hamza, "The effect of sulfurisation temperature on structural properties of $CuAlS_2$ thin films," *IOSR J. Appl. Phys.* **3**(1), 12–17 (2013).
96. J. Olejníček et al., "$CuIn_{1-x}Al_xS_2$ thin films prepared by sulfurization of metallic precursors," *J. Alloys Compd.* **509**(41), 10020–10024 (2011).
97. R. Brini et al., "Study of the growth of $CuAlS_2$ thin films on oriented silicon (111)," *Thin Solid Films* **517**(7), 2191–2194 (2009).
98. M. Abaab, A. S. Bouazzi, and B. Rezig, "Competitive $CuAlS_2$ oxygen gas sensor," *Microelectron. Eng.* **51**, 343–348 (2000).
99. S. M. Ahmad, "Study of structural and optical properties of quaternary $Cu_xAg_{1-x}AlS_2$ thin films," *Optik* **127**(20), 10004–10013 (2016).
100. M. Caglar, S. Ilican, and Y. Caglar, "Structural, morphological and optical properties of $CuAlS_2$ films deposited by spray pyrolysis method," *Opt. Commun.* **281**(6), 1615–1624 (2008).
101. R. Woods-Robinson et al., "Combinatorial tuning of structural and optoelectronic properties in $Cu_xZn_{1-x}S$," *Matter* **1**(4), 862–880 (2019).
102. R. Woods-Robinson et al., "P-type transparent Cu-alloyed ZnS deposited at room temperature," *Adv. Electron. Mater.* **2**(6), 1500396 (2016).
103. R. Woods-Robinson et al., "Wide band gap chalcogenide semiconductors," arXiv:1910.08153 (2019).
104. A. M. Diamond et al., "Copper-alloyed ZnS as a p-type transparent conducting material," *Phys. Status Solidi A* **209**(11), 2101–2107 (2012).
105. L. Wei et al., "Machine learning optimization of p-type transparent conducting films," *Chem. Mater.* **31**(18), 7340–7350 (2019).
106. S. K. Maurya et al., "High figure-of-merit p-type transparent conductor, Cu alloyed ZnS via radio frequency magnetron sputtering," *J. Phys. D Appl. Phys.* **50**(50), 505107 (2017).
107. T. T. Thanh et al., "Synthesis and photocatalytic application of ternary Cu-Zn-S nanoparticle-sensitized TiO_2 nanotube arrays," *Chem. Eng. J.* **210**, 425–431 (2012).
108. F. Di Benedetto et al., "Electrodeposited semiconductors at room temperature: an x-ray absorption spectroscopy study of Cu-, Zn-, S-bearing thin films," *Electrochim. Acta* **179**, 495–503 (2015).
109. D. E. Ortíz-Ramos, L. A. González, and R. Ramirez-Bon, "P-type transparent Cu doped ZnS thin films by the chemical bath deposition method," *Mater. Lett.* **124**, 267–270 (2014).
110. M. Dula, K. Yang, and M. Ichimura, "Photochemical deposition of a p-type transparent alloy semiconductor Cu_xZn_yS," *Semicond. Sci. Technol.* **27**(12), 125007 (2012).
111. K. Yang and M. Ichimura, "Fabrication of transparent p-type Cu_xZn_yS thin films by the electrochemical deposition method," *Jpn. J. Appl. Phys.* **50**(4), 040202 (2011).
112. K. Ishikawa et al., "Preparation and electrical properties of (LaO)AgS and (LnO)CuS (Ln = La, Pr, or Nd)," *J. Electrochem.* **138**(4), 1166–1170 (1991).
113. M. Palazzi et al., "Crystal structure and properties of (LaO) CuS and (LaO) AgS," *The Rare Earths in Modern Science and Technology* 347–350, Springer, Boston, Massachusetts (1982).
114. K. Ueda et al., "Transparent p-type semiconductor: LaCuOS layered oxysulfide," *Appl. Phys. Lett.* **77**(17), 2701–2703 (2000).
115. H. Hiramatsu et al., "Fabrication of heteroepitaxial thin films of layered oxychalcogenides LnCuOCh (Ln = La–Nd; Ch = S–Te) by reactive solid-phase epitaxy," *J. Mater. Res.* **19**(7), 2137–2143 (2004).

116. D. O. Scanlon et al., "Understanding doping anomalies in degenerate p-type semiconductor LaCuOSe," *J. Mater. Chem. C* **2**(17), 3429–3438 (2014).
117. M.-L. Liu et al., "A promising p-type transparent conducting material: layered oxysulfide $[Cu_2S_2][Sr_2Sc_2O_5]$," *J. Appl. Phys.* **102**(11), 116108 (2007).
118. E. Hildebrandt et al., "Controlled oxygen vacancy induced p-type conductivity in HfO_{2-x} thin films," *Appl. Phys. Lett.* **99**(11), 112902 (2011).
119. K.-H. Xue et al., "Prediction of semimetallic tetragonal Hf_2O_3 and Zr_2O_3 from first principles," *Phys. Rev. Lett.* **110**(6), 065502 (2013).
120. T. Kim et al., "Material design of new p-type tin oxyselenide semiconductor through valence band engineering and its device application," *ACS Appl. Mater. Interfaces* **11**(43), 40214–40221 (2019).
121. F.-L. Schein, H. von Wenckstern, and M. Grundmann, "Transparent p-CuI/n-ZnO heterojunction diodes," *Appl. Phys. Lett.* **102**(9), 092109 (2013).
122. D. Chen et al., "Growth strategy and physical properties of the high mobility p-type cui crystal," *Cryst. Growth Des.* **10**(5), 2057–2060 (2010).
123. C. S. Herrick and A. D. Tevebaugh, "Oxygen-controlled conduction in thin films of cuprous iodide: a mixed valency anion semiconductor," *J. Electrochem. Soc.* **110**(2), 119–121 (1963).
124. K. Bädeker, "Über eine eigentümliche Form elektrischen Leitvermögens bei festen Körpern," *Ann. Phys.* **334**(8), 566–584 (1909).
125. Y. Kumashiro, "Refractory semiconductor of boron phosphide," *J. Mater. Res.* **5**(12), 2933–2947 (1990).
126. M. Iwami, T. Tohda, and K. Kawabe, "Crystal growth of boron mono-phosphide and its electrical and optical properties," *IEEJ Trans. Fundam. Mater.* **95**(5), 216–222 (1975).
127. Y. Youn et al., "Large-scale computational identification of p-type oxide semiconductors by hierarchical screening," *Chem. Mater.* **31**(15), 5475–5483 (2019).
128. N. Sarmadian et al., "Easily doped p-type, low hole effective mass, transparent oxides," *Sci. Rep.* **6**, 1–9 (2016).
129. P. M. Sirimanne and V. P. S. Perera, "Progress in dye-sensitized solid state solar cells," *Phys. Status Solidi B* **245**(9), 1828–1833 (2008).
130. S. Villain et al., "Electrical properties of CuI and the phase boundary Cu|CuI," *Solid State Ionics* **76**(3–4), 229–235 (1995).
131. O. Ohtaka et al., "Ionic conductivities of CuI phases at high pressures and temperatures," *J. Phys. Soc. Jpn.* **79**(Suppl. A), 51–53 (2010).
132. A. N. Gruzintsev and V. N. Zagorodnev, "Change in optical properties of CuI crystals upon annealing in vacuum," *Phys. Solid State* **54**(1), 117–122 (2012).
133. D. Kim et al., "Thermal-strain-induced splitting of heavy- and light-hole exciton energies in CuI thin films grown by vacuum evaporation," *Phys. Rev. B* **60**(19), 13879–13884 (1999).
134. Y. Peng et al., "Efficient organic solar cells using copper(I) iodide (CuI) hole transport layers," *Appl. Phys. Lett.* **106**(24), 243302 (2015).
135. R. Heasley et al., "Vapor deposition of transparent, p-type cuprous iodide via a two-step conversion process," *ACS Appl. Energy Mater.* **1**(12), 6953–6963 (2018).
136. S. J. Clarke et al., "Structures, physical properties, and chemistry of layered oxychalcogenides and oxypnictides," *Inorg. Chem.* **47**(19), 8473–8486 (2008).
137. M. Morales-Masis et al., "Conductance switching in Ag_2S devices fabricated by *in situ* sulfurization," *Nanotechnology* **20**(9), 095710 (2009).
138. H. Lin et al., "Growth of environmentally stable transition metal selenide films," *Nat. Mater.* **18**(6), 602–607 (2019).
139. A. Jain et al., "The materials project: a materials genome approach to accelerating materials innovation," *APL mater.* **1**(1), 011002 (2013).
140. T. S. Tripathi and M. Karppinen, "Atomic layer deposition of p-type semiconducting thin films: a review," *Adv. Mater. Interfaces* **4**(24), 1700300 (2017).
141. R. Eason, *Pulsed Laser Deposition of Thin Films. Applications-Led Growth of Functional Materials*, John Wiley & Sons, Inc., Hoboken (2007).

142. C. Stock and E. E. McCabe, "The magnetic and electronic properties of oxyselenides: influence of transition metal ions and lanthanides," *J. Phys. Condens. Matter* **28**(45), 453001 (2016).

Angela N. Fioretti received her PhD in materials science from Colorado School of Mines in 2017. Her graduate work focused on combinatorial development of ternary nitride semiconductors for photovoltaics. Currently, she is a Marie Curie postdoctoral fellow at the Ecole Polytechnique Fédérale de Lausanne in Switzerland, working on development of novel carrier selective contact materials for solar cells.

Monica Morales-Masis received her PhD from Leiden University, Netherlands in 2012. From 2012 to 2017 she was at the Photovoltaics Laboratory (PVLab) of the Ecole Polytechnique Federale de Lausanne (EPFL), Switzerland as team leader for its transparent conducting oxides activities. Since 2018, she is an assistant professor at the University of Twente, Netherlands, focusing on synthesis and study of optoelectronic materials, such as transparent conducting oxides, sulfides and halide perovskites for photovoltaics and applications beyond.